Spatial Bunching of Entangled Four Photons

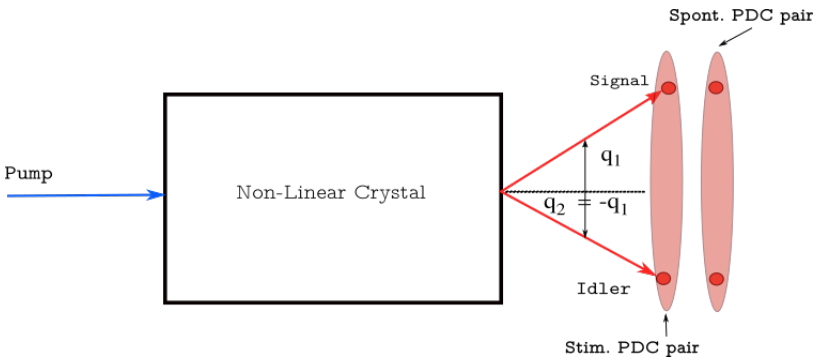

THESIS

submitted in partial fulfillment of the
requirements for the degree of

MASTER OF SCIENCE
in
PHYSICS

Author :	Snigdh Sabharwal
Student ID :	s1729063
Supervisor :	Michiel De Dood
2^{nd} corrector :	Martin Van Exter

Leiden, The Netherlands, June 2, 2017

Spatial Bunching of Entangled Four Photons

Snigdh Sabharwal

Huygens-Kamerlingh Onnes Laboratory, Leiden University
P.O. Box 9500, 2300 RA Leiden, The Netherlands

June 2, 2017

Abstract

We observe spatial bunching of four spatially entangled photons produced by parametric down-conversion in a single periodically poled KTP crystal. This effect involves an increased probability to generate all four photons in the same optical mode. To observe the effect we create entangled double pairs at 826 nm wavelength using a 5 mm long crystal and investigate their correlations by measuring three-fold coincidence counts. We demonstrate that two-fold and three-fold coincidence measurements are sufficient to experimentally distinguish a spatially entangled two-photon state from a four-photon state and a four-photon state from a six-photon state, respectively. This makes experimental observation of the effect feasible at moderately high pump-powers.

Contents

Chapter 1

Introduction

Entanglement has been and still remains one of the key concepts that has made the study quantum mechanics so counter-intuitive and challenging. Ever since the emergence of the EPR article [1], quantum entanglement has been at the forefront of scientific research until this day. Over the years due to continued progress and investigation, it made possible for many groundbreaking experiments that at some point were thought to be experimentally unrealizable. A beautiful review of some of those can be found in the following ([2] [3]).
In this thesis, we will be investigating the entanglement of photons and using it to explore their spatial bunching. By spatial bunching one simply refers to the probability of finding two or more photons at the same spatial position being larger than them being found at different positions. The first-ever experimental demonstration of bunching of photons was observed by Hanbury-Brown and Twiss [4] in 1956. Over the years many such experiments ([2] [5] [6]) have been performed but none to the best of our knowledge has been performed to explore the spatial bunching of (spatially) entangled four photons, where all the four photons are generated using a single PDC source. The work presented in this thesis builds on the previous works of a PhD student [7]. She was the first one to actually observe the two fold-coincidences of both the entangled pair and a double pair, but was however unable to explain these correlations. In this thesis, we will be exploring the spatial correlations of four photons in a three-fold coincidence experiment. In order to understand the experimentally observed correlations, we have also developed a general theoretical framework which was previously missing.
This thesis has been structured in the following way: We first begin by introducing the non-linear process of Parametric Down Conversion (PDC),

that generates the spatially entangled photons and introduce the theoretical framework needed to analyze and make predictions about the two and three-fold coincidence experiments in Chapter 2. Chapter 3 describes our experimental setup followed by a brief discussion of the results. In Chapter 4 we conclude with a quick overview of what we acheived in this thesis and suggest a possible direction one can look to explore in the future. We also provide some extra information as Appendices 1,2 and 3 if the reader so deems it necessary.

Chapter 2

Theory

In this chapter we briefly touch upon the non-linear process of Parametric Down Conversion (PDC) used to generate entangled photon pairs followed by an introduction of the down-converted state corresponding to the generated spatially entangled photon pairs in our experiment. We then introduce the biphoton wavefunction and the phase-mismatch which lays the groundwork for understanding the meaning of entanglement in a more formal sense. We then derive the correlation functions by making use of the free space field operator, to explore and investigate the two-fold and three-fold coincidences.

2.1 Parametric-Down Conversion

Parametric-Down Conversion (PDC) or more commonly known as Spontaneous PDC (See Fig 2.1) is a second-order non-linear process where input *pump* photons are split into pairs of output photons, conventionally known as *signal* and *idler*, which can be correlated in polarization, transverse momentum, arrival time and/or frequency. The experimental configuration considered in this thesis aims to create photons entangled in their spatial degree of freedom (transverse momenta) for a fixed identical polarization. In order to achieve this, one needs to take the time correlation of the down-converted photons into account, i.e. one needs to ensure that the detection time window is smaller than the correlation time of the down-converted photons. The process of PDC has been extensively studied over the years and we refrain from a detailed discussion here.The interested reader may however refer to ([2], [3], [8])

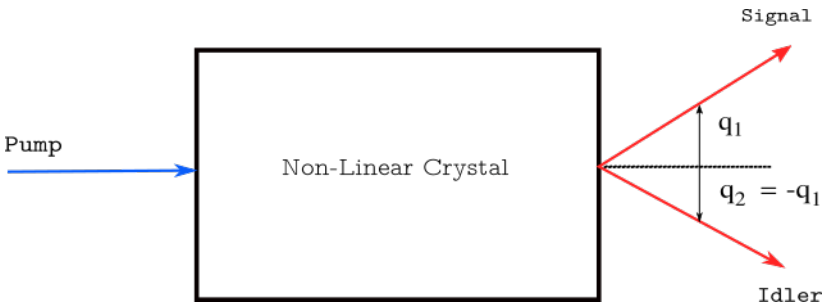

Figure 2.1: *Parametric-Down Conversion*

While the PDC process leads to the generation of pairs of spatially entangled photons, it is by no means limited to the production of just one pair. In principle, multiple pairs can be generated but reaching this regime is experimentally challenging as laser intensities close to damage thresholds of the material are often required. In addition, efficient generation of pairs critically depends on how well one can phase-match the pump and down-converted photons. Before addressing the specific details of phase-matching in Section 2.4 we will introduce general expressions for the quantum state of PDC in Section 2.2 and the connected bi-photon wavefunction in Section 2.3.

2.2 The PDC State

In general, the down-converted state in the Heisenberg picture, can be obtained by the action of the operator, $\exp\left(-\frac{i}{\hbar}\int \hat{H}_{int}(t)dt\right)$ on the vacuum state and then using perturbation theory to obtain a series expansion ([2],[3],[8]) up to the required order, depending on how many spatially entangled pairs one is interested in. Here $\hat{H}_{int}(t)$ refers to the non-linear interaction Hamiltonian. The down-converted state up to two pairs is given by,

$$|\psi\rangle^{PDC} = A\,|vac\rangle + B\int d\{\alpha\}\,\phi\{\alpha\}\,|\alpha\rangle + C\int d\{\alpha,\beta\}\,\phi\{\alpha\}\,\phi\{\beta\}\,|\alpha,\beta\rangle \tag{2.1}$$

where we introduce the following shorthand notation to emphasize the mathematical structure of the state.
$\{\alpha\} \equiv (\vec{q_1},\vec{q_2})$, $\{\beta\} \equiv (\vec{q_3},\vec{q_4})$, $\quad d\{\alpha\} \equiv d\vec{q_1}d\vec{q_2}$, $\quad \phi\{\alpha\} \equiv \phi(\vec{q_1},\vec{q_2})$, $|\alpha\rangle \equiv |\vec{q_1},\vec{q_2}\rangle$
The coefficients A, B and C are given by
$A \equiv 1 - B^2\Gamma - 12C^2\Gamma^2$, $\qquad C = B^2/2$, $\qquad \Gamma = \int d\{\alpha\}\,|\phi\{\alpha\}\,|^{2*}$, and
$\vec{q_i}$ corresponds to the transverse momenta wavector of the i-th PDC photon.
$\phi(\vec{q_1},\vec{q_2})$ is the biphoton wavefunction that will be introduced futher in Section 2.3

The first term here corresponds to the vacuum state, the second term is the first order perturbation term corresponding to a single PDC pair or the **two-photon state** and the last term is the next higher order term corresponding to the double PDC pair or the **four-photon state**.

This state with no explicit dependence on frequency, is typically valid under the condition that the spectral bandwidth of the PDC photons is smaller than their respective frequencies i.e., $\Delta\omega \ll \omega$, allowing one to ignore the frequency correlations of the down-converted field. This situation is typically achieved by using narrow-band spectral filters. For the purposes of this thesis, we will be working with a more general state and include the frequency degree of freedom using

$$\{\alpha\} \equiv (\vec{q_1},\Omega_1,\vec{q_2},\Omega_2)$$

*$\Gamma = 1$ throughout this thesis [5]

in Eqn. [2.1]. Here, $\vec{q_1}, \Omega_1$ corresponds to a down-converted photon with transverse momenta $\vec{q_1}$ and detuned frequency $\Omega_1 = \tilde{\omega}_1 - \frac{\omega_p}{2}$.
In this thesis, we will refer to Eqn. 2.1 (for $\{\alpha\}$ as defined above) as the down-converted state, unless stated otherwise.

2.3 Biphoton-Wavefunction

The biphoton wavefunction is extremely important in understanding the concept of spatial entanglement of the PDC photons. The ideas here will be used and extended to understand two and three-fold coincidences that can be observed experimentally. Spatial entanglement can be understood from the fact that the biphoton wavefunction is **non-factorizable** that is, $\phi(\vec{q_1}, \vec{q_2}) \neq f(\vec{q_1}) \cdot h(\vec{q_2})$ [Eqn. 2.2] which naturally leads to the **non seperability** of the down-converted state [Eqn. (2.1)]. If $|\psi\rangle = \sum_{i,j} \phi(q_i, q_j) |q_i, q_j\rangle$ and $\phi(q_i, q_j) \neq f(q_i) \cdot h(q_j)$ then, $|\psi\rangle$ is entangled : $|\psi\rangle \neq \sum_i f(q_i) |q_i\rangle \otimes \sum_j h(q_j) |q_j\rangle$.
For parametric-downconversion, the bi-photon wavefunction upto a constant is given by,

$$\phi(\vec{q_1}, \vec{q_2}) \equiv \exp\left(-\frac{w_p^2}{4}|\vec{q_1} + \vec{q_2}|^2\right) \operatorname{sinc}\left(\frac{\Delta k_z L}{2}\right) \tag{2.2}$$

where,
w_p is the pump beam size
$\Delta k_z = k_{p_z} - k_{s_z} - k_{i_z}$ is the phase-mismatch along the propagation direction of the pump , with
$k_{j_z} = \sqrt{k_j^2 - \vec{q_j}^2}$ the z-component of propagation vector, $j = p, s(1), i(2)$
$k(\omega_j) = \frac{n(\omega_j, T)\omega_j}{c}$ is the magnitude of the propagation vector
ω_j is the frequency of the j-th field
$n(\omega_j, T)$ is the corresponding refractive index
c is the speed of light
L is the length of the crystal along the z-direction.

Eqn. 2.2 is a product of the spatial distribution of the pump field (which we assumed to be gaussian) times a function that takes into account the effects of the crystal length and phase-mismatch on the process of parametric down conversion. Throughout this thesis we will be assuming that the down-converted fields are **degenerate**, i.e have the same frequency ω and the pump has a central frequency, $\omega_p = 2\omega$.
To keep the analysis more general we do not trace out the frequency label of the PDC field. Under such a condition the biphoton wavefunction upto a constant is given by,

$$\phi(\vec{q_1}, \Omega_1, \vec{q_2}, \Omega_2) = \exp\left(-\frac{w_p^2}{4}|\vec{q_1} + \vec{q_2}|^2 - \left(\frac{\Omega_p}{2\sigma}\right)^2 \right) \mathrm{sinc}(\frac{\Delta k_z L}{2}) \tag{2.3}$$

where,
$\Omega_p = \tilde{\omega} - \omega_p$ is the detuning from the central frequency of the pump[†]
$\Omega_j = \tilde{\omega} - \omega_j$ is the detuned frequency of the PDC field $(j = 1, 2)$ and
σ is the frequency spread of the pump beam

In this thesis, we will refer to Eqn. 2.3 as the biphoton-wavefunction, unless stated otherwise.
It is important to consider the complete biphoton wavefunction given by Eqn. 2.3. In the experiment, narrow band filters will be employed to trace out the frequency content of the two-photon field. The complete expression allows one to quantify how narrow the filter should be and keep track of spatial correlations induced by spectral filtering. The equations that we derive for the two and three-fold coincidences can in principle be applied to cases when one does not use such tight spectral filtering. In that case, however, one needs to modify the phase-mismatch in order to incorporate the effects of wide-band spectral filters [Eqn. 2.6].

[†]Here we have assumed the following $\Omega_p = \Omega_1 + \Omega_2$.

2.4 Phase-Matching

For non-linear processes to be efficient, phase-matching conditions need to be satisfied. These conditions ensure that light produced by the non-linear process at each position in the crystal interferes constructively at the exit of the crystal. This condition fixes the phase relationship between the pump and the PDC photons, and requires matching the momenta of the interacting photons over the entire length of the crystal, so that $\Delta k_z = 0$. However because of refractive-index dispersion $[n(2\omega, T) \neq n(\omega, T)]$ inside the crystal , phase-matching conditions are generally not satisfied. [See Fig. 2.2 and 2.3]

For the collinear case (see Fig. 2.2), the phase-mismatch is given by

$$\Delta k_{coll} = k(2\omega, T) - 2k(\omega, T) = \frac{2\omega}{c}[n(2\omega, T) - n(\omega, T)] \neq 0 \quad (2.4)$$

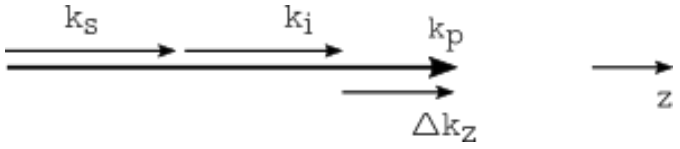

Figure 2.2: *Collinear Phase-Mismatch*

For the non-collinear case (see Fig. 2.3),

$$\Delta k_z = k_{p_z} - k_{s_z} - k_{i_z} \neq 0 \quad (2.5)$$

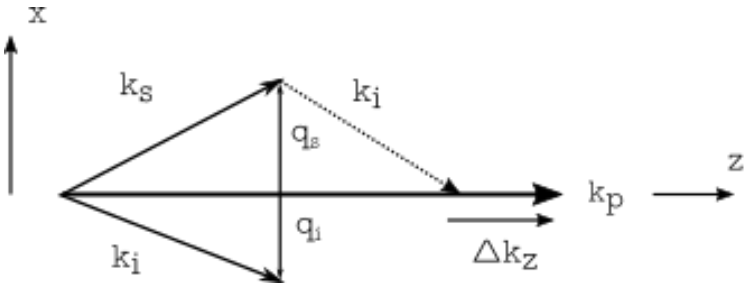

Figure 2.3: *Non-Collinear Phase-Mismatch*

To phase-match the non-linear interaction one can use the anisotropy (birefringence) of the crystal to find a special angle (termed as the phase-matching

angle) where the polarization dependence of the refractive index of the pump and the down-converted field [9] compensates the effect of refractive index dispersion. An alternative is to periodically modulate the non-linear coefficient d, such that phase mismatch between the pump and the PDC field is compensated by a reciprocal lattice vector. The latter type of Phase-Matching is often referred to as Quasi-Phase Matching (QPM), while the former is commonly termed as Birefringent Phase-Matching (BPM). In our experiments, we make use of periodically-poled KTP crystals and QPM.

2.4.1 Quasi-Phase Matching

QPM allows for phase-matching for a *specific* $\Delta k_z \neq 0$. As previously mentioned, we want to achieve phase-matching over the entire length of the crystal, but due to phase-mismatch, there is a finite coherence length ($l_c = \frac{\pi}{\Delta k_z}$) over which the pump and PDC photons build-up a phase difference of π. In (first-order) QPM one introduces a periodic structure [Fig. 2.4] inside the crystal of poling period $\Lambda = 2l_c$ such that the non-linear coefficient d periodically flips sign. The result is that the pump and the PDC photons are brought back in phase due to the inversion of d. Mathematically, the periodic poling of the non-linear coefficent leads to a generation of an additional phase factor quantified by a vector $K = \frac{2\pi}{\Lambda}$ in k space (Fourier Domain). This modifies the effective phase-mismatch to $\Delta\tilde{k}_z = \Delta k_z - K$ [Fig. 2.5,Fig. 2.6]. By appropriately choosing the poling period (Λ), one can obtain $\Delta\tilde{k}_z \sim 0$.

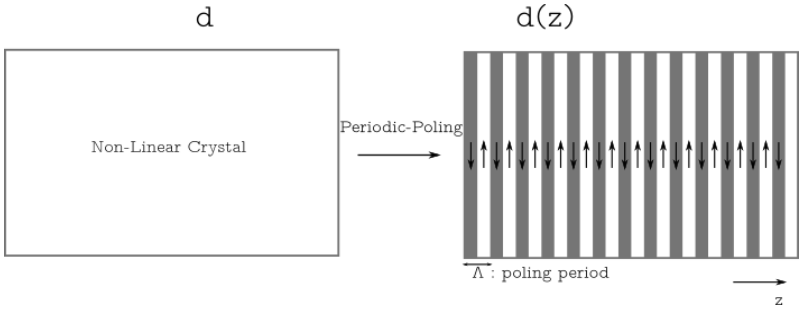

Figure 2.4: *Periodic Poling*

For non-collinear QPM [Fig. 2.5], one finds that

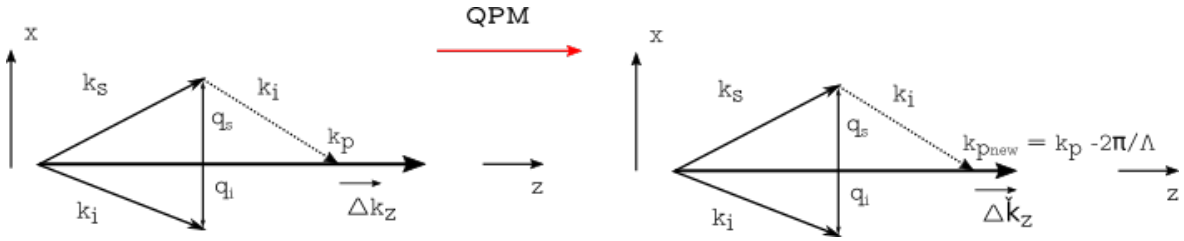

Figure 2.5: *Non-Collinear Quasi-Phase Mismatch*

$$\Delta\tilde{k}_z = \Delta\tilde{k}_{coll} + D_+\Omega_p + \left[\frac{D_p''\Omega_p^2}{2} - \frac{D''(\Omega_1^2+\Omega_2^2)}{2}\right] + \left[\frac{|\vec{q_1}|^2+|\vec{q_2}|^2}{2k(\omega,T)} - \frac{|\vec{q_p}|^2}{2k(2\omega,T)}\right] \tag{2.6}$$

where,
$\Delta\tilde{k}_{coll} \equiv k_{p_{new}} - k(2\omega,T) = \Delta k_{coll} - K$
Ω_j is the detuning from the central frequency of the j-th field $(j = p,1,2)$.
$D_+ = c|\frac{1}{v_g(2\omega)} - \frac{1}{v_g(\omega)}|$ is the walk-off parameter
$D'' = \frac{d^2k}{d\tilde{\omega}^2}\Big|_{\tilde{\omega}=\omega}$ corresponds to the dispersion of PDC field [10]
$D_p'' = \frac{d^2k}{d\tilde{\omega}^2}\Big|_{\tilde{\omega}=2\omega}$ corresponds to the dispersion of the pump beam, and
$\vec{q_p} = \vec{q_1} + \vec{q_2}$ is the transverse momentum wavevector of the pump beam

Eqn. 2.6 was obtained by Taylor expanding k in terms of Ω and q, i.e. using

$$k_{z_j} \approx k_j + k_j'\Omega_j + \frac{k_j''\Omega_j^2}{2} - \frac{|\vec{q_j}|^2}{2k_j} \qquad j = p,1,2 \tag{2.7}$$

We stress that Eqn. 2.7 is only valid under the paraxial approximation ($k_z \approx k - \frac{q^2}{2k}$) and for narrow-band filtering of the PDC light. [refer: X entanglement]

The first term in Eqn. 2.6 $\Delta\tilde{k}_{coll}$ times $L/2$ [Eqn. 2.8] refers to the collinear-phase mismatch and depends on temperature. This phase mismatch can be approximated by ([11], [7], [12])

$$\frac{\Delta\tilde{k}_{coll}L}{2} \equiv \phi_{coll}(\omega,T) = \frac{L\omega}{c}\left[c_1(T-T_{pm}) + c_2\left((T-T_o)^2 - (T_{pm}-T_o)^2\right)\right] \tag{2.8}$$

This parameter controls the opening angle of the PDC beam as a function of temperature. The Temperature $T = T_{pm}$ is referred to as the Phase-Matched Temperature where $\phi_{coll}(\omega, T) = 0$, corresponding to collinear-phase matching. For the PPKTP crystal and the wavelength used in our experiment this typically occurs at $T \sim 60°C$ [Fig. 2.6]. At any other T, $\phi_{coll}(\omega, T) \neq 0$.

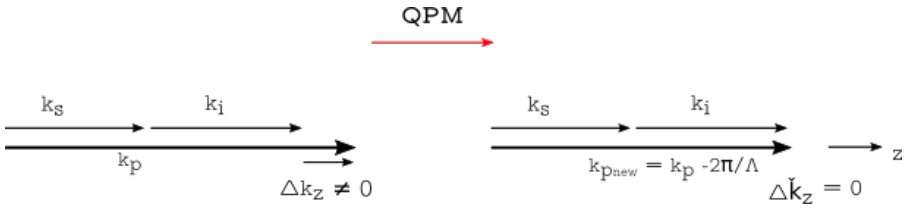

Figure 2.6: *Collinear Quasi-Phase-Matching*

The second and third term (in square brackets) in Eqn. 2.6 take into account the fact that we have a pulsed pump and allows one to investigate the effects of dispersion of the pump and the PDC field on spatial entanglement[‡]. The fourth term in the square brackets is responsible for the spatial correlations among the down-converted photons. This term tells us that the down-converted photons are spatially anticorrelated i.e., $q_1 \approx -q_2$. It is these correlations that we wish to explore in this thesis, in the context of single and double pairs.

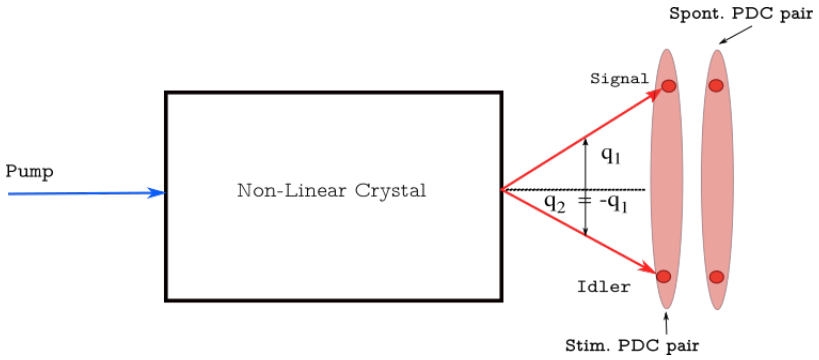

Figure 2.7: *Schematic drawing illustrating the processes of Spontaneous and Stimulated PDC*

[‡]We will not be investigating these details in this thesis

2.5 Entangled Four-Photons or Two-Independent pairs?

So what exactly does entanglement mean in the four-photon case? We know that by the non-linear interaction of the pump beam with the crystal we can generate entangled two photons but what does an 'entangled double-pair' mean? A reasonable first guess would be an extension of the definition of entanglement to a double pair, that is to say if one detected a photon with transverse momenta q_1, then there is a finite possibility to detect two photons with transverse momenta $q_2 \approx -q_1$ and the fourth photon with a transverse momenta q_1 being the same as the first one. However, these correlations are identical to those of two 'independent' spatially entangled pairs accidently created in the same mode. The only way to distinguish these different contributions is via the statistics i.e., in their respective generation probabilities. An entangled double pair is more likely to be generated as opposed to two independent double pairs due to the process of stimulated emission. This is best illustrated by considering the double pairs generated in the time domain. In this case the following relation holds[13],

$$P_4 = \frac{P_2^2(1+\chi)}{2} \tag{2.9}$$

where,
P_4 is the probability of creating four photons within a single pump pulse duration
P_2 is the probability of creating two photons within a single pump pulse duration
$\chi = \frac{r}{(1+r^2)^{1/2}} \in [0,1]$ is termed as the 'Visibility' parameter, which is a measure of the distinguishability of the created photons defined by the ratio, r between the coherence time (Δt_{coh}) of the created photons and the duration of the pump pulse (τ_p), i.e. $r = \frac{\Delta t_{coh}}{\tau_p}$.

The fact that whether the created double pair is entangled or independent is characterized by the visibility parameter. For $\chi = 0$, all photons are independent double pairs produced by a spontaneous emission process, whereas, for $\chi = 1$, the photons are entangled double pairs, effectively doubling the probability to create four photons. In the latter process, the second pair is often referred to as the **Stimulated PDC** [Fig. 2.7].

We mentioned the pairs being 'independent' but its exact meaning still remains unclear. By an independent pair we mean a state (in a discrete mode) of the following kind $|\psi\rangle_{indep} = |1_q \bowtie 1_{-q}\rangle \otimes |1_q \bowtie 1_{-q}\rangle$. [§] It is these pairs that we refer to as the independent double pairs and deemed as unwanted background, that we correct for in our experiment [See Sec. 3.1.1]. An example of a correlated double pair would be the following $|\psi\rangle_{corr} = |1_q \bowtie 1_{-q} \bowtie 1_q \bowtie 1_{-q}\rangle = |2_q \bowtie 2_{-q}\rangle$. What differentiates the independent double pairs from the correlated ones is the fact that the two independent pairs are time separable (temporally distinguishable) or put differently belong to two different temporal modes. For instance, two spatially entangled single pairs created by two different pump pulses would be considered as being independent double pairs. A correlated double pair, on the other hand, is in the same temporal mode and it is these correlated double pairs that we wish to observe and understand. There exists a slight subtlety in what exactly we mean by a temporal mode here, as there exists not one but a spread Δt, imposed by the finite bandwidth of the spectral filter $\Delta\tilde{\omega}$. This $\Delta t = \Delta t_{coh}$ is often referred to as the coherence time of the PDC photons. Due to this, there exists a finite possibility that allows for the independent pairs to be in the same 'temporal mode' as well. This contribution of two independent pairs in the same temporal mode has a two times lower detection probability [Eqn. 2.9] as compared to an entangled double pair that is also temporally indistinguishable.
Until now we have only heuristically looked at the problem of spatial entanglement of two and four photons. While this has its benefits, it does not allow one to make any predictions in the coincidence experiments that we set-up. To compare our experimental results to theory we need to compute correlation functions. Having completely defined our (PDC) state, our aim is to derive expressions corresponding to the two and three-fold coincidence experiments. For that, we need operators corresponding to the observables in our experiment. In the next section, we define our free space field operator, needed to set-up the proper groundwork to derive the correlation functions.

[§]We introduce the $\bowtie$ symbol as a mathematical notation for the term 'Join' (for us 'Entangled') to remind ourselves that the pair itself is correlated.

2.6 Field Operator

In order to evaluate the correlation functions, we need to find the operators corresponding to the basis in which we detect the down-converted state. In our case, we detect the PDC state in the momentum basis defined through the position of the detectors in the far-field of the PDC source. Assuming the PDC beam to be nearly monochromatic (which can be justified by the use of narrow band-pass filters), one can define the (detection) field operator to be,

$$\hat{E}(\vec{r},t) \propto \int d\Omega d\vec{k} e^{i(\vec{k}.\vec{r}-\Omega t)} \hat{a}(\vec{k},\Omega) \tag{2.10}$$

where $\hat{a}(\vec{k},\Omega)$ is the annihilation operator in the continuum mode.
However, this operator is ill-suited for the problem of field propagation and needs to be slightly modified to allow for free space propagation. Under the paraxial approximation, the field operator after propogating a distance z is given by,

$$\hat{E}(\vec{\rho},z,t) \propto e^{i(kz)} \int d\Omega d\vec{q} e^{i(\vec{q}.\vec{\rho}-\frac{q^2 z}{2k}-\Omega t)} \hat{a}(\vec{q},\Omega) \tag{2.11}$$

where $\vec{\rho} = (x,y)$.
In the experiment, the detector moves along the x-direction to collect the light produced by the PDC source. Therefore, we restrict the discussion to a 1D version of the equation above.

$$\hat{E}(x,z,t) \equiv \frac{1}{2\pi} \int dq d\Omega f_{spec}(\Omega) f_{spat}(q) e^{i(qx-\frac{q^2 z}{2k}-\Omega t)} \hat{a}(q,\Omega) \tag{2.12}$$

where $q = q_x$.
Here, we have introduced the functions f_{spec} and f_{spat} as the transmission of the spectral and spatial filters corresponding to the band-pass filter and the Single Mode Fiber (SMF) we use in the experiment. We assume these to be approximately Gaussian.

Having found the field operator, we will next try and find the correlation functions which will help us in understanding coincidences that we measure experimentally. Note that, due to the introduction of the filters f_{spec} and f_{spat}, the product of the spectral and spatial filters with the Eqn. 2.3 is what we will be refering to as the biphoton wavefunction.

2.7 Correlation Function

Correlation functions should be interpreted as the conditional probability of detecting photons in the basis in which one detects and are given by the expectation values of normally ordered field operators acting on the quantum state for the system under consideration [14].

2.7.1 Second-Order Correlation Function

The second-order or one-photon (Intensity) correlation function describes the probability of detecting a photon as a function of the detector's position (x) located at the detection plane,z at some t. It is given by,

$$G^{(1)}(x,z,t) = \langle \hat{E}^{\dagger}(x,z,t)\hat{E}(x,z,t)\rangle = ||\hat{E}(x,z,t)\,|\psi\rangle\,||^2 \tag{2.13}$$

In the experiment we work with the configuration as shown in Fig. 2.8 to detect singles and the two-fold coincidences. The only degree of freedom that the detectors have is in the x-direction at some fixed, z constraining $z = z1 = z2$. In the experiment this distance z is ideally defined as the focal distance of the lens used to collect the PDC photonsand the detectors are placed at the same distance from the lens to collect the photons in the far-field.

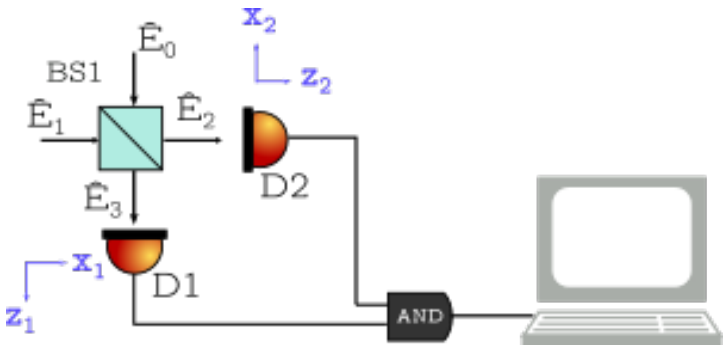

Figure 2.8: *Coincidence Configuration for measuring the Intensity (singles) and two-fold coincidences using a beamspitter BS1 and detectors (D1 and D2). The output of the detectors is fed into a logical AND gate which are then counted by a computer*

We use the standard beam-splitter transformation equations [3] to relate the field operators before and after the beam splitter.

$$\hat{E}_2 = \sqrt{T}\hat{E}_1 - \sqrt{R}\hat{E}_0 \tag{2.14}$$

$$\hat{E}_3 = \sqrt{R}\hat{E}_1 + \sqrt{T}\hat{E}_0 \tag{2.15}$$

where,
$\hat{E}_2$ and $\hat{E}_3$ represent **output port field operators** and
$\hat{E}_0$ and $\hat{E}_1$ are the **input port field operators**.
T and R are the intensity transmission and reflection coefficients of the beam splitter.
We find the second-order correlation function at the output port 3 of the beamsplitter to be given by

$$\begin{aligned} G^{(1)}(x_1, z_1, t_1) =& \langle \hat{E}_3^{\dagger}(x_1, z_1, t_1) \hat{E}_3(x_1, z_1, t_1) \rangle \qquad (2.16) \\ =& (S_2^{\mathrm{I}} + S_4^{\mathrm{I}}) \int dq_2 d\Omega_2 \left| \Theta^{2D}(x_1, z_1, t_1, q_2, \Omega_2) \right|^2 + \\ & S_4^{\mathrm{II}} \int dq_2 d\Omega_2 \Theta^{(1)}(x_1, z_1, t_1, q_2, \Omega_2) \Theta^{(2)}(x_1, z_1, t_1, q_2, \Omega_2) \qquad (2.17) \end{aligned}$$

where
$S_2^{\mathrm{I}} = 2R|B|^2$, $S_4^{\mathrm{I}} = 8R|C|^2\Gamma$, and $S_4^{\mathrm{II}} = 16R|C|^2$ are constants corresponding to the two and four-photon state respectively. The functions $\Theta^{(1)}$, $\Theta^{(2)}$ and Θ^{2D} are defined as

$$\Theta^{(1)}(x_1, z_1, t_1, q_2, \Omega_2) \equiv \int dq_1 d\Omega_1 \Theta^{2D}(x_1, z_1, t_1, q_1, \Omega_1) \left[\phi(q_1, \Omega_1, q_2, \Omega_2) \right]^* \qquad (2.18)$$

$$\Theta^{(2)}(x_1, z_1, t_1, q_2, \Omega_2) \equiv \int dq_1 d\Omega_1 \left[\Theta^{2D}(x_1, z_1, t_1, q_1, \Omega_1) \right]^* \phi(q_1, \Omega_1, q_2, \Omega_2) \qquad (2.19)$$

$$\Theta^{2D}(x_1, z_1, t_1, q_2, \Omega_2) \equiv \frac{1}{2\pi} \int d\Omega_1 dq_1 e^{i(q_1 x_1 - \Omega_1 t_1)} \left[\phi(q_1, \Omega_1, q_2, \Omega_2) e^{-\frac{i q_1^2 z_1}{2k_p}} \right] \qquad (2.20)$$

Eqn. 2.20 is the 2D fourier-transform of the biphoton wavefunction times a phase, $e^{-\frac{i\vec{q}^2 z}{2k}}$ that depends on the detector's longitudnal distance, z from the crystal. One can likewise determine the correlation function of the output port 2 of the beam splitter. To arrive at Eqn. 2.17 we make use of the following state

$$|\psi\rangle = |\psi\rangle^{PDC} \otimes |vac\rangle \tag{2.21}$$

where $|\psi\rangle^{PDC}$ [Eqn. 2.1] is input at port 1 and the vacuum state $|vac\rangle$ is input at port 0 of the beam-splitter. We remind the reader that the continuous variable description has operators that obey the following algebra,

$$[\hat{a}(q_1, \Omega_1), \hat{a}^\dagger(q_2, \Omega_2)] = \delta(q_1 - q_2)\delta(\Omega_1 - \Omega_2) \tag{2.22}$$
$$\hat{a}(q, \Omega)\,|vac\rangle = 0 \tag{2.23}$$

where the operators are normalized to the dirac delta function.

2.7.2 Fourth-Order Correlation Function

The fourth-order or two-photon (field) correlation function describes the probability of detecting two-fold coincidences between two-detectors [Fig. 2.8] positioned at (x_1) and (x_2), located at detection planes, z_1 and z_2 at times t_1 and t_2 respectively.

$$G^{(2)}(x_1, z_1, t_1, x_2, z_2, t_2) = ||\hat{E}_2(x_2, z_2, t_2)\hat{E}_3(x_1, z_1, t_1)\,|\psi\rangle\,||^2 \quad (2.24)$$

Going through the same steps as we did for the second-order correlation function, we find that the fourth-order correlation function is given by,

$$\begin{aligned} &G^{(2)}(x_1, z_1, t_1, x_2, z_2, t_2) = (D_2^{\mathrm{I}} + D_4^{\mathrm{I}})\Big|\Theta^{4D}(x_1, z_1, t_1, x_2, z_2, t_2)\Big|^2 + \\ &D_4^{\mathrm{II}}\left[\int dq_2 d\Omega_2 |\Theta^{2D}(x_1, z_1, t_1, q_2, \Omega_2)|^2 . \int dq_1 d\Omega_1 |\Theta^{2D}(x_2, z_2, t_2, q_1, \Omega_1)|^2\right] + \\ &D_4^{\mathrm{II}}\int dq_2 d\Omega_2 \Theta^{2D}(x_1, z_1, t_1, q_2, \Omega_2)\left[\Theta^{2D}(x_2, z_2, t_2, q_2, \Omega_2)\right]^* \end{aligned} \quad (2.25)$$

where,
$D_2^{\mathrm{I}} = 2TR|B|^2$, $D_4^{\mathrm{I}} = 8TR\Gamma|C|^2$ and $D_4^{\mathrm{II}} = 8TR|C|^2$

$$\Theta^{4D}(x_1, x_2, z_1, z_2, t_1, t_2) \equiv \frac{1}{4\pi^2}\int d\{\alpha\}\, e^{i(q_1x_1 + q_2x_2 - \Omega_1t_1 - \Omega_2t_2)}\left[\phi\{\alpha\}\, e^{-i(\frac{q_1^2 z_1}{2k_p} + \frac{q_2^2 z_2}{2k_p})}\right] \quad (2.26)$$

with $\{\alpha\} \equiv (q_1, \Omega_1, q_2, \Omega_2)$

Eqn. 2.26 is the 4D Fourier transform of the biphoton-wavefunction modulated by a phase term that depends on the distance of the detectors, z_1 and z_2 from the crystal.

The 'Independent' Two-Fold Coincidence Function

Owing to the choice of our pump pulse duration we have the possibility of generating independent double pairs that might contribute to the two-fold coincidences. However, our aim from the start has been to explore and quantify correlations coming from pairs generated by stimulated emission only. In the experiment [See Sec. 3.1.1] the contribution from independent pairs produced by spontaneous emission is subtracted by measuring coincidences between events in different laser pulses. Here we evaluate this independent contribution to the coincidence experiment. This is an important step to compare our theoretical correlations with the experimentally observed ones. The independent two-fold coincidences are given by a product of the second-order correlation functions of detectors D1 and D2 respectively, i.e.

$$G^{(2)}_{ind}(x_1, x_2, z_1, z_2, t_1, t_2) = G^{(1)}(x_1, z_1, t_1).G^{(1)}(x_2, z_2, t_2) \tag{2.27}$$

The real or the net two-fold coincidences are therefore the difference between Eqn. 2.25 and Eqn. 2.27

$$G^{(2)}_{net}(x_1, z_1, x_2, z_2) = 2G^{(2)}(x_1, z_1, 0, x_2, z_2, 0) - G^{(2)}_{ind}(x_1, x_2, z_1, z_2, 0, 0) \tag{2.28}$$

The fact that we have set $t_1 = t_2 = 0$ ns is imposed by the way we have set up our experiment [See Sec. 3.1.1] using an electronic time delay. The factor of 2 is a result of the fact that the coincidences obtained correspond to the case when the relative time delay between D1 and D2 is zero. This occurs when the measured coincidences arise from a pulse at 0 ns and another from a pulse at τ_p. The coincidences so measured for a pulse at 0 ns and those measured at τ_p are indistinguishable from each other [13], which adds a factor of 2 in Eqn. 2.28.

2.7.3 Sixth-Order Correlation Function

The sixth-order or three-photon correlation function describes the probability of detecting three-fold coincidences between three-detectors [Fig. 2.8] positioned at (x_1), (x_2) and (x_3), located at detection planes, z_1 , z_2 and z_3 and at times t_1, t_2 and t_3 respectively.

$$G^{(3)}(x_1, x_2, x_3, z_1, z_2, z_3, t_1, t_2, t_3) = ||\hat{E}_2'(x_3, z_3, t_3)\hat{E}_3'(x_2, z_2, t_2)\hat{E}_3(x_1, z_1, t_1)\,|\psi\rangle\,||^2 \tag{2.29}$$

A possible three-fold coincidence configuration similar to the experimental setup, is shown in the figure below.

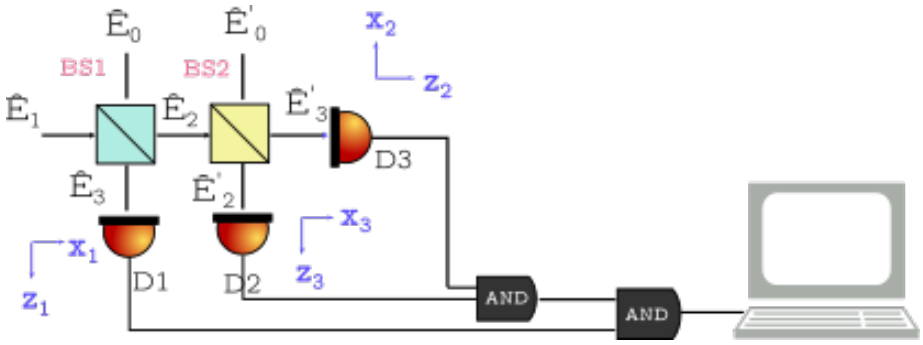

Figure 2.9: *Possible experimental configuration to measure the three-fold coincidences using two beamsplitters BS1 and BS2. The output of the detectors (D1, D2 and D3) is fed into two logical AND gates and coincidences are counted with a computer*

To calculate the correlation function we use the following beam-splitter transformation for the operators,

$$\hat{E}_2 = \sqrt{T}\hat{E}_1 - \sqrt{R}\hat{E}_0 \tag{2.30}$$
$$\hat{E}_3 = \sqrt{R}\hat{E}_1 + \sqrt{T}\hat{E}_0 \tag{2.31}$$
$$\hat{E}_2' = \sqrt{R_1}\hat{E}_2 - \sqrt{T_1}\hat{E}_0' \tag{2.32}$$
$$\hat{E}_3' = -\sqrt{R_1}\hat{E}_0' + \sqrt{T_1}\hat{E}_2 \tag{2.33}$$

where T,R and T_1,R_1 are the intensity transmission and reflection coefficients of beamsplitters 1 (BS1) and 2 (BS2), respectively.

Repeating the same steps as before, we find that the sixth-order correlation function is given by,

$$G^{(3)}(x_1,x_2,x_3,z_1,z_2,z_3,t_1,t_2,t_3) = 8|C|^2R_1T_1RT^2... \\ \Big[|\Theta^{4D}(x_1,x_2,z_1,z_2,t_1,t_2)|^2\int dq_4 d\Omega_4|\Theta^{2D}(x_3,t_3,z_3,q_4,\Omega_4)|^2 \\ +|\Theta^{4D}(x_1,x_3,z_1,z_3,t_1,t_3)|^2\int dq_4 d\Omega_4|\Theta^{2D}(x_2,t_2,z_2,q_4,\Omega_4)|^2 \\ +|\Theta^{4D}(x_2,x_3,z_2,z_3,t_2,t_3)|^2\int dq_4 d\Omega_4|\Theta^{2D}(x_1,t_1,z_1,q_4,\Omega_4)|^2\Big] \tag{2.34}$$

In the experiment we use a slightly different three-fold configuration as shown in the figure below. Instead of moving detectors D2 and D3, we move the input port (port a in Fig. 2.10) of the Single Mode Fiber (SMF) Beamsplitter while keeping the detectors fixed as shown in the figure.

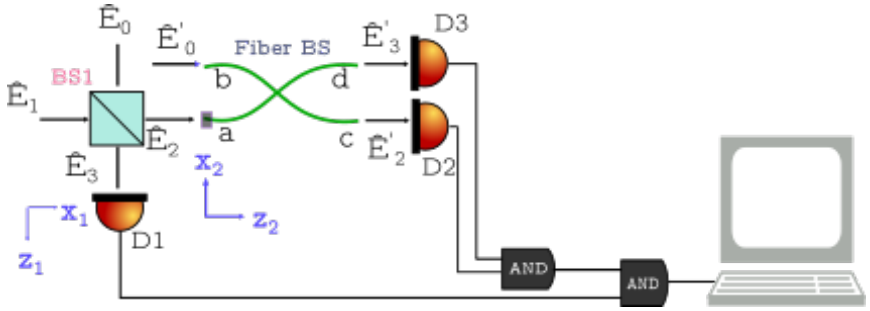

Figure 2.10: *Experimental Three-Fold Coincidence Configuration where one beamsplitter is replaced by a fiber based beamsplitter*

This configuration imposes the constraint $x_2 = x_3$. Furthermore, we set up the experiment such that $t_2 = t_3$ and $z_1 = z_2 = z_3 \equiv z$.

In this case the sixth-order correlation function simplifies to,

$$G^{(3)}(x_1,x_2,z,t_1,t_2) = 8|C|^2R_1T_1RT^2 \\ \Big[2|\Theta^{4D}(x_1,x_2,z,t_1,t_2)|^2\int dq_4 d\Omega_4|\Theta^{2D}(x_2,t_2,z,q_4,\Omega_4)|^2 + \\ |\Theta^{4D}(x_2,x_2,z,t_2,t_2)|^2\int dq_4 d\Omega_4|\Theta^{2D}(x_1,t_1,z,q_4,\Omega_4)|^2\Big] \tag{2.35}$$

The 'Independent' Three-Fold Coincidence Function

Similar to the case of the two-fold coincidences, we also have a contribution from independent pairs to the three-fold coincidences. This independent contribution can be evaluated as a product of the two-fold coincidence between detectors D2 and D3 times the intensity/second-order correlation function corresponding to detector D1 [See Fig. 2.10]. In the experiment (like in the two-fold case) this independent contribution is measured and subtracted using the delay line unit [See Chap. 3]. The independent three-fold coincidences are given by,

$$G^{(3)}_{ind}(x_1, z_1, t_1, x_2, z_2, t_2, x_3, z_3, t_3) = G^{(2)}(x_2, z_2, t_2, x_3, z_3, t_3).G^{(1)}(x_1, z_1, t_1) \tag{2.36}$$

which under the constraints $x_2 = x_3$, $t_2 = t_3$ and $z_1 = z_2 = z_3 \equiv z$ becomes

$$G^{(3)}_{ind}(x_1, t_1, x_2, t_2, z) = G^{(2)}(x_2, t_2, x_2, t_2, z).G^{(1)}(x_1, t_1, z) \tag{2.37}$$

The real or the net three-fold coincidences is therefore a difference between Eqn. 2.35 and 2.37.

$$G^{(3)}_{net}(x_1, x_2, z) = 2G^{(3)}(x_1, x_2, z, 0, 0) - G^{(3)}_{ind}(x_1, x_2, z, 0, 0) \tag{2.38}$$

Chapter 3

Experiment

In this chapter we present and discuss the results of the two and three-fold coincidence experiments. We find that the laser induced damage, known as gray-tracking ([15], [16]) is the main limitation to future experiments and include a section on this phenomenon at the end of the chapter.

3.1 Setup

3.1.1 The Two-fold Coincidence Experiment

In our experiment, spatially entangled photons are generated by the non-linear interaction of the pump beam with a PPKTP (periodically poled KTP*) crystal. The crystals are provided by Raicol and have a length $L = 5$ mm for a poling period $\Lambda = 3.675$ μm, unless stated otherwise. In order to investigate the fourth-order correlation (two-fold coincidences) of such photons we used the setup as shown in Fig. 3.1. The setup consists of a frequency-doubled pulsed Ti: Sapphire laser which outputs a pump pulses at a wavelength $\lambda = 413.2$ nm with a pulse duration of ~ 2 ps, at a repetition rate of 80 MHz. The pump beam is fed into a beam expander [12], used to adjust the width of the pump beam inside the non-linear crystal (NLC). We chose a setting such that the Gaussian pump beam's FWHM inside the NLC is 70 ± 1 μm. The beam is guided by the mirrors (M1) and (M2) via a lens (L1, f1 = 250 mm) which focuses the pump beam inside the NLC. PDC photons, centered around a wavelength of 826.4 nm are generated in the process and are selected by appropriate optical filters. The NLC (PPKTP) crystal is placed on a mount that is temperature controlled

*KTP: potassium titanyl phosphate (KTiOPO4)

to tune the phase matching in PPKTP, and control the opening angle of the PDC beam.
To separate the pump beam from the PDC photons an anti-reflection coated Gallium-phosphide wafer (GaP) is placed after the crystal allowing only the PDC photons to pass. The PDC photons are thereafter filtered by a 1 nm FWHM bandpass filter (F),and collected in the far-field detection plane by a lens (L2, f2 = 250 mm), placed exactly 250 mm behind the crystal.

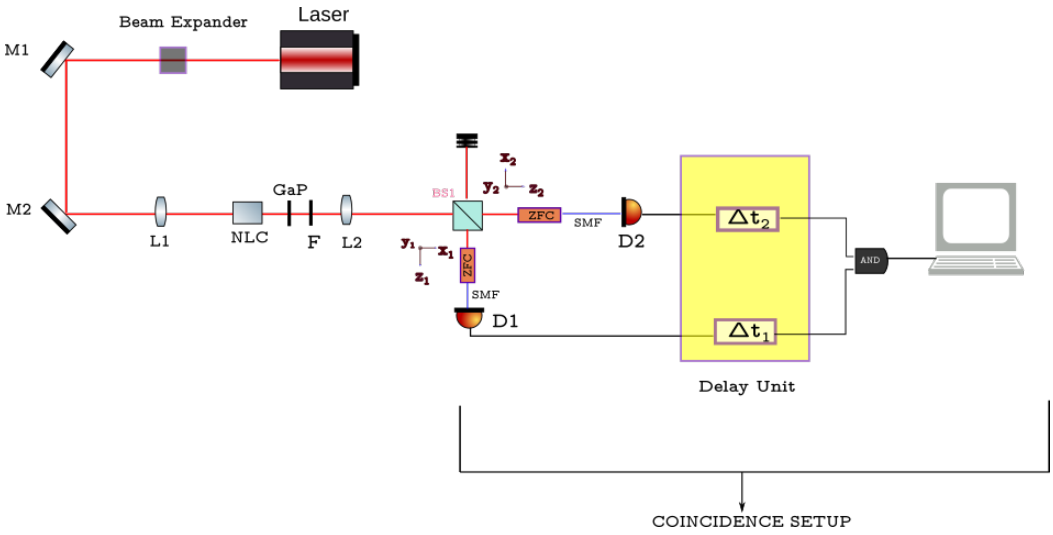

Figure 3.1: *Schematic outline of the experimental setup that we used to measure the two-fold coincidences.*

In order to find the spatial correlations between the entangled photons, we use the coincidence scheme as shown in Fig. 3.1. The entangled pair(s) are sent through one of the input ports of the 50:50 Beam Splitter (BS1) to a zoom-fiber collimator (ZFC) model number $ZC618SMA\text{-}B$, used to collect and collimate the PDC beam. We set the zoom to 18 mm in all our experiments. These ZFCs are placed on a computer controlled translation stage allowing for collection in the x,y plane at a fixed z. In our experiment, the ZFCs are placed equidistantly in the exact far-field of the PDC source (267.5 mm after L2) correcting for the optical thickness of the large $2''$ cube beamsplitter (BS1). The beam is collected into a single-mode-fiber (SMF) with a 5 μm mode diameter and analyzed by the single-photon detectors (D1) and (D2), respectively.

The counts from these detectors are sent to an AND-gate (having a detection time window of 5ns [†]) via a delay line unit. These delay lines are

[†]chosen so that only those entangled photons generated within a single pump pulse duration are detected.

used as a means to differentiate the correlated photons from the independent ones generated in a single pump pulse. This is done by measuring the coincidences (AND-gate counts) for two different pulses i.e., measuring the coincidences when both $\Delta t_1 = \Delta t_2 = 0$ ns and then doing the same for $\Delta t_2 = 0$ ns , $\Delta t_1 = 12$ ns [‡].The actual coincidence is recorded as the difference between the two.
The major difference in this setup as opposed to previous experiments [12] is that instead of using multimode fibers (MMF) we used single-mode fibers (SMF). This is a crucial step since the measurement of three-fold coincidences (which we will see later on) is much more sensitive to the alignment of the setup as opposed to two-fold coincidences. The large (50 μm) diameter of MMFs gives a false sense of alignment, greatly complicating the three-fold coincidence experiment. Hence, a collective decision was made to switch to SMFs and avoid MMFs.

3.1.2 Results

Figure 3.2 shows false colour plots of the measured (left) and calculated two-fold coincidence rate (right) on a natural logarithmic scale as a function of position x_1 and x_2 (in mm) [See Fiq. 3.1]. Both plots are corrected for independent pairs by subtracting the coincidence rate with $\Delta t_1 = 12$ ns. The experimental data was obtained by focussing the laser beam inside the crystal at an average power of 133 mW and for a crystal temperature $T = 61.25°C$. The theory plot was obtained by taking the natural logarithm of the absolute value of Eqn. 2.28.

3.1.3 Discussion

There are a couple of things one can learn from Fig. 3.2. Let's first consider the case when an incoming pump photon generates a single spatially entangled pair. For the coincidence set-up shown in Fiq. 3.1 this entangled two-photon state is detected when detectors D1 and D2 click for the ZFCs positioned at x_1 and $x_2 = -x_1$ respectively. This is what we have as described before as an entangled pair, with photons entangled in their spatial degree of freedom. This contribution is easily visible both in the experimental and the theoretical plot along the anti-diagonal, $x_2 = -x_1$. The fact that we see a spread around $x_2 = -x_1$ as opposed to sharp lines is because of the spread in transverse momenta q as a result of the finite spectral and spatial bandwidth of the pump pulse. Next, consider the case

[‡]The pump pulses have a temporal separation of 12ns.

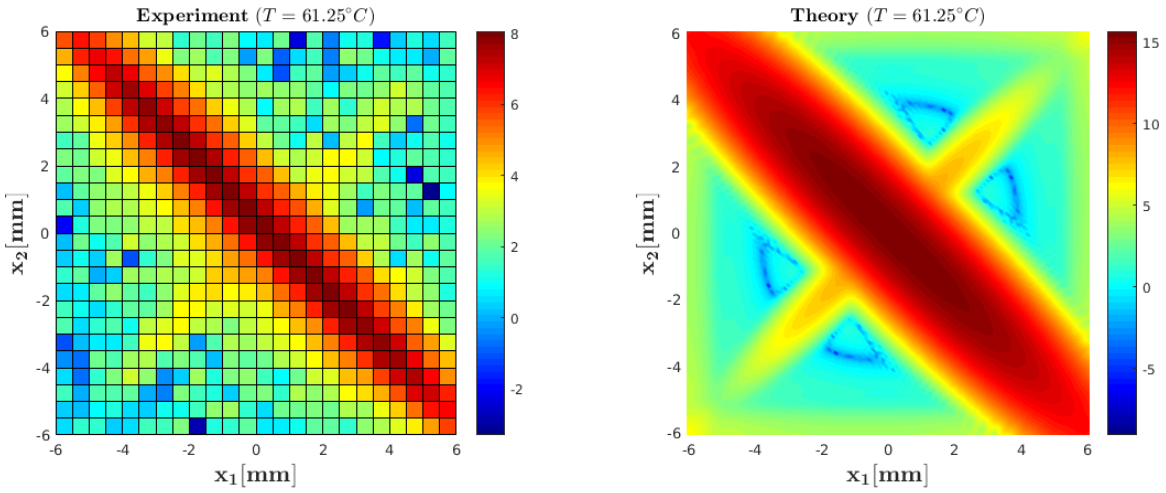

Figure 3.2: *Experimentally obtained two fold coincidence rate at $T = 61.25°C$ for a laser power of 133mW (left). Corresponding theoretically two-fold coincidences (right)*

when an incoming pump photon generates an entangled double pair. It should be easy to see that the four-photon state would be recorded not just along the anti-diagonal but also along the diagonal. The anti-diagonal corresponds to the case when two of the entangled four photons leads to a coincidence between D1 and D2 for oppositely positioned ZFCs. The diagonal on the other hand corresponds to the case when the two photons have the same transverse momenta and hence are detected at the same positions $x_1 = x_2$ of the ZFCs. This latter contribution is clearly visible in both the theory and the experiment. It is important to note that the two photons detected by the detectors along the anti-diagonal for the two-fold coincidence setup, cannot be distinguished as being either from an entangled pair or the double pair whereas along the diagonal the only possible two photons are from the entangled double pair. The picture sketched here remains valid as long as the power of pump beam is low enough to neglect the generation of more than an entangled double pair in the nonlinear process.

3.1.4 The Three-fold Coincidence Experiment

The experimental setup for measuring the three-fold coincidences is essentially the same as the setup for detecting two-fold coincidences. Instead of having a SMF connected to D2, we now replace the SMF by a 50:50 (2x2) Single-Mode Fiber Beamsplitter (SMFBS). The PDC beam (via the ZFC) is now input into one of the input ports of the SMFBS. The output ports of the SMFBS are then connected to the Single-Photon Detectors (D2) and (D3) respectively. The detectors D2 and D3 are connected to an additional AND-gate via a delay line unit whose output is connected to the input of another AND-gate (as shown in the Fig. 3.3). The other input to this AND-gate is the output of D1 via the delay line.

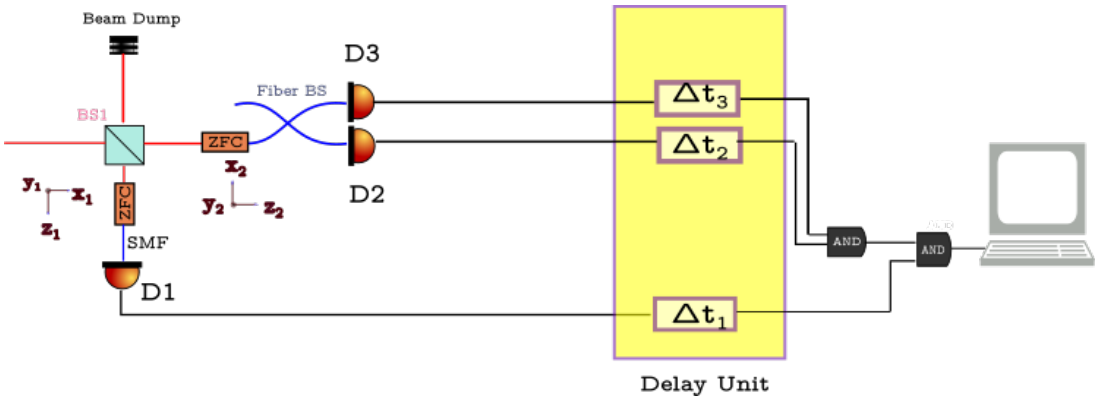

Figure 3.3: *Experimental setup to measure the three-fold coincidences. Photons are collected by zoom fiber collimators (ZFC) and detected by single photon detectors (D1-D3). Three-fold coincidence are generated by two concatenated AND gates.*

3.1.5 Result

Fiqures 3.4 and 3.5 summarize results obtained for three-fold coincidences at two different crystal temperatures of $61°C$ and $59°C$, respectively. The experimental data (left figures) was obtained for an average pump power of 80 mW. The plots on the right of the same figures correspond to their theoretical counterparts obtained using Eqn. 2.38. Fiqure 3.6 shows the experimental three-fold coincidences (red circles) obtained by summing along the rows of the figures shown in 3.4 and 3.5. The black curve is the corresponding theoretical fit obtained by making use of the equations shown in [Appendix 1] with the crystal temperature, T_{theory} as the only free parameter. The pump beam waist, pulse duration and temperature

dependence of the phase mismatch are determined by other independent experiments. The fits were obtained by first normalizing both the theory and experiment to one and then later on scaling them by the experimentally obtained counts per second. We do this primarily because we are interested only in the shape of the three-fold coincidences. The constant that we scale by is to only give the reader an idea about the three-fold coincidence count rate in our experiment.

3.1.6 Discussion

In the three-fold coincidence experiment, we expect to observe coincidences coming from an entangled double pair along the anti-diagonal of the coincidence plot (as shown in Fig. 7.1). Let's consider the case when the pump photon leads to the generation of an entangled double pair. Detectors D2 and D3 (see Fig. 3.3) detect photons in the same mode collected by the input of the fiber beam splitter. This constrains the three-fold coincidences to cases when two photons, having the same transverse momenta are detected at D2 and D3. This leaves only the possibility that the photon detected at D1 will have a transverse momentum opposite to the ones detected at D2 and D3[§]. The central peak is due to the fact that the four photons are spatially bunched, i.e. all four photons are in the same spatial mode with $q = 0$ and inturn become spatially indistinguishable. A good fit is obtained for the experiment at $T = 61^{\circ}C$ with the fitted temperature close to the experimental value. The quality of the fit for the data at $59^{\circ}C$ is comparable, but we observe a large difference ($\sim 1.5^{\circ}C$) between the fit parameter T_{theory} and the temperature in the experiment. We attribute this to a gradual change in the properties of the PPKTP crystal due to laser induced damage, a phenomenon known under the name gray tracking ([15], [16]). We observe that gray-tracking changes the phase-matching in PPKTP and shifts the phase-matching temperature T_{pm} by a few degrees. Being the main limitation to future experiments with PPKTP, we discuss the process of gray-tracking in section 3.1.7.
From the observed count rates for single photons and coincidence count rates one can estimate the detection efficiency and the number of pairs porduced. We find single count rates of $\sim 1.7 \times 10^3$ sec^{-1} mW $^{-1}$ nm^{-1} for detector D1 and $\sim 8.6 \times 10^2$ sec^{-1} mW $^{-1}$ nm^{-1} for detectors D2 and D3. From this we estimate detection efficiencies of 1.5% for detector D2 and D3 and 2.9% for detector D1. The number of pairs generated by the crystal is approximately 5.85×10^4 sec$^{-}1$ mW $^{-1}$ nm^{-1} from which we obtain a sin-

[§]The entangled photons are anti-correlated i.e., $q_2 = -q_1$

gle pass gain $\kappa t \approx 7.3 \times 10^{-4}$ mW^{-1} nm^{-1}, i.e. a single pass gain of 0.073 is obtained at 100 mW pump power, comparable to earlier studies [7]. The three-fold coincidences are expected to be a factor $(\kappa t)\eta$ smaller than the two-fold coincidence rate, where η is the detection efficiency. At 120 mW pump power we observe approximately 3000 two-fold coincidences and expect a 3-fold coincidence rate to be around 3.1 sec^{-1}.

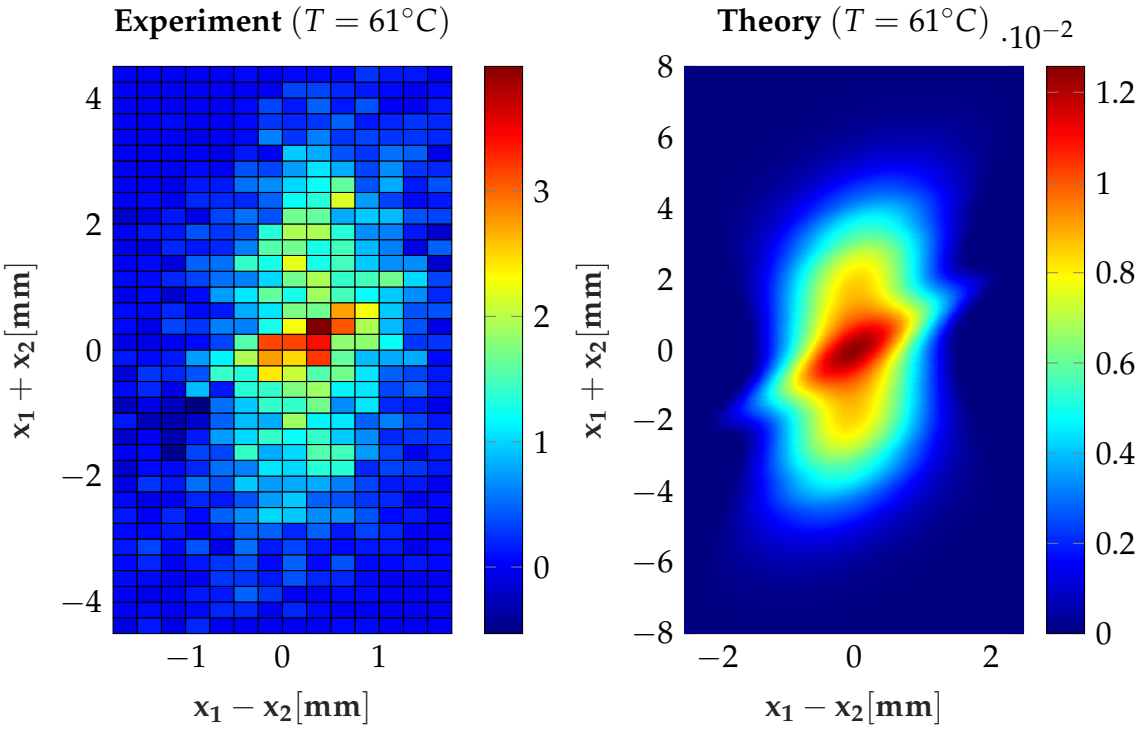

Figure 3.4: *The figure on the left is the experimentally obtained three-fold coincidences at $T = 61°C$ for a laser power of 80 mW and the one on the right is the corresponding theoretical prediction at the same temperature.*

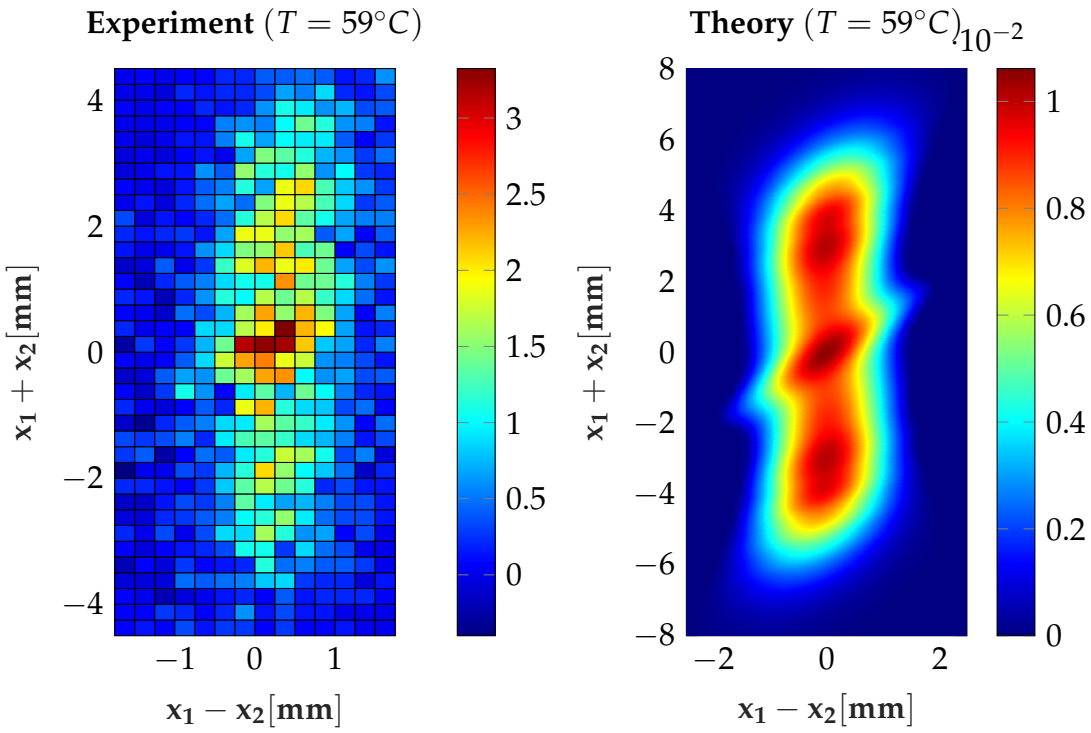

Figure 3.5: *Three-fold coincidences (Experimental and theoretical) obtained for $T = 59°C$. The experimental data was obtained at 80 mW of pump power.*

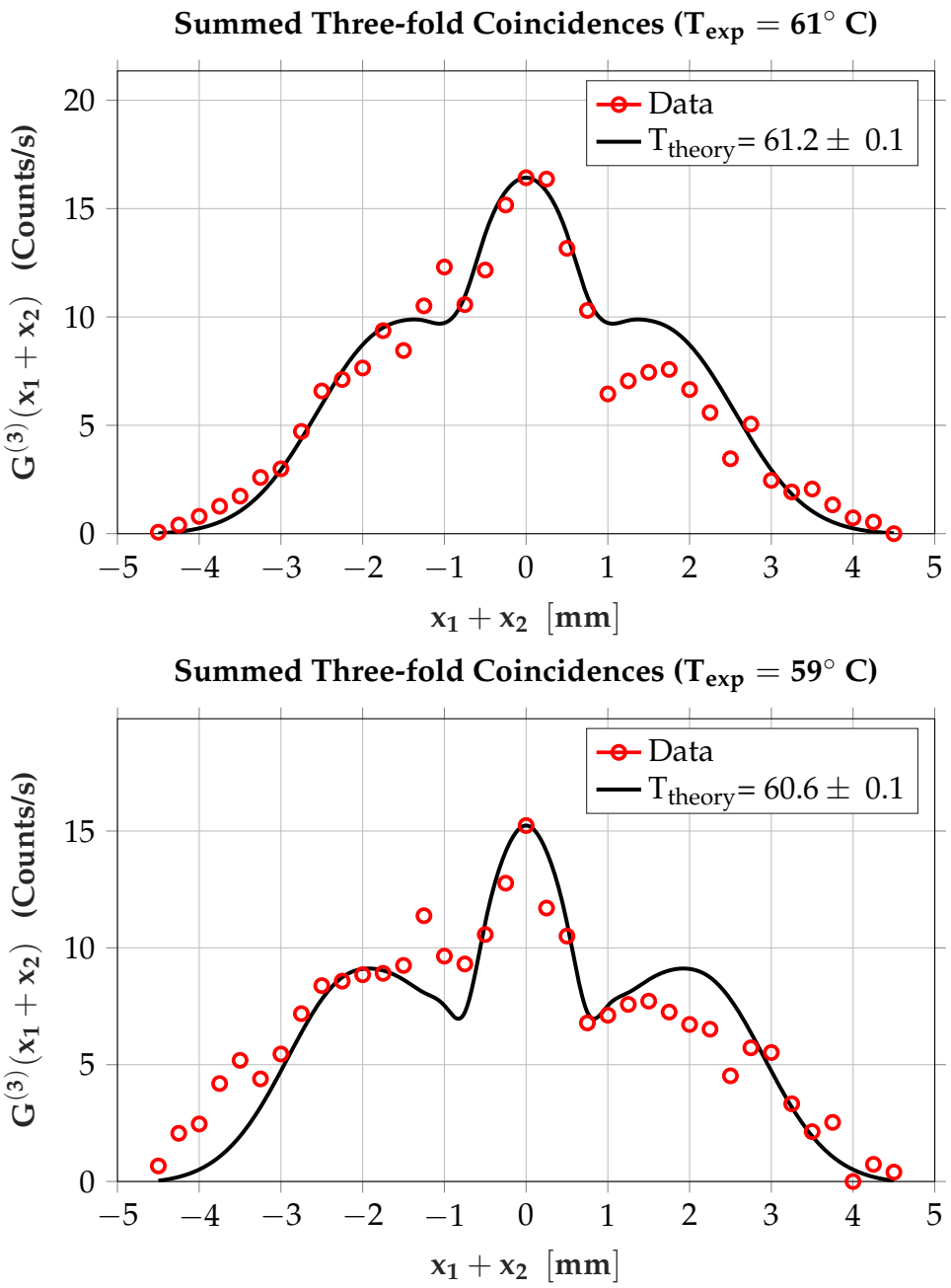

Figure 3.6: *Three-fold coincidence at $T = 61°C$ (top) and $T = 59°C$ (bottom) obtained by summing along the rows of the three-fold coincidences in Fig. 3.4 and 3.5 (red symbols). The black lines are fits to the data with the temperature T_{theory} as the free parameter.*

3.1.7 Gray-Tracking

The main problem while working with the PPKTP crystal, is that in order to generate double pairs, one needs to pump it with intensities close to the damage threshold of the crystal. This in return causes gray-tracking or photodarkening of the crystal induced by the laser light. Gray-tracking refers to the absorption of photons in the crystal at wavelengths in the range $400 - 600$ nm. As a result one typically observes a dark-grey spot in the crystal. One of the effects of gray-tracking is that it changes the phase-matching in the crystal. This causes a gradual shift of the phase-matching temperature with time which is also seen in our experiment. A common way to reverse gray-tracking is by annealing the crystal. For our 2 mm crystal (as shown in the Fig. 3.7 and 3.8), we annealed it at $130^{\circ}C$ C for about 3 months. While this visibly removes the gray tracks, it doesn't improve the transmission at the pump wavelength. Possible reasons for this could be the fact that we are not annealing the crystal at sufficiently high temperatures or sufficiently long enough. Although the mechanism of gray-tracking is not clear, the effect depends on the amount of the pump power absorbed in a given area inside the crystal. Initially this might be due to the two-photon absorption. Once the gray track is formed, the drop in transmission is noticeable on a time scale of several hours for an average pump power of 140 mW, a pump pulse duration of 2 ps and a FWHM of 20 μm. Note that this translates to a peak power per squared centimetre of around 65.4 $\mathrm{MW/cm^2}$ which is still an order of magnitude smaller than the damage threshold of the crystal, 600 $\mathrm{MW/cm^2}$ (as per raicol specs [17]). We find that gray tracking sets in more rapidly at higher intensities, greatly complicating the experiments in that regime.

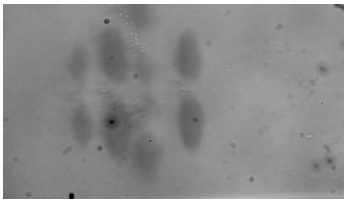

Figure 3.7: *Microscope image of the 2 mm crystal showing several gray tracks in the material.*

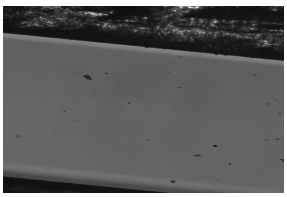

Figure 3.8: *Microscope image of the 2 mm crystal after annealing at* $130^{\circ}C$ *for 3 months.*

Chapter 4

Conclusion

In this thesis we have showed the spatial bunching of entangled four-photons. To observe the spatial bunching of the double pair, we had to ensure that the pairs were not temporally distinguishable. This was experimentally achieved by measuring the three-fold coincidences for the same pulse and for two adjacent pulses and then taking the difference of the two. By doing so we ensure that we do not take into account the contribution of 'independent' pairs to the three-folds. We have showed that tracing out the frequency contribution is a good approximation in cases of narrow-band spectral filtering. This is visible in the quality of the fits we produced for the three-fold coincidences that make use of correlation functions where we trace out the frequency contribution of the field. Also through our experiment we showed that one can differentiate a two photon state from a four photon state in the two-fold coincidences and the four photon state from a six photon state in the three-fold coincidences subject to the laser powers so used.
While the use of PPKTP allows us to control the bunching of the photons by adjusting the crystal temperature, it also shows gray-tracking at the high laser intensities required to generate multiple pairs. One could in principle work at low pump power for which four photons are generated in the non-linear process, with the drawback being that one has to wait longer to obtain the experimental data. At this moment it is unclear if gray tracking can be prevented and if there is a real advantage of lower powers to gray tracking as well. There is a need for a detailed analysis on how one can bypass or get rid (if possible) of gray-tracking if one wants to investigate multi-photon entanglement with PPKTP. A possible future direction one could look to explore is the how the walk-off and dispersion parameters, $D_{+}$and $D^{''}$, of the PDC field affects the fourth order correla-

tions at the two photon level. This one can do by the equations we so derived in the theory chapter of this thesis.

Chapter 5

Appendix 1

Here we briefly introduce the three-fold correlation functions that we use for numerically fitting the data. The approach we will be using is based on tracing out the frequency contribution to PDC, which is a good approximation for the case of narrow-band filters. The PDC state for such a case is the one defined in Eqn.[2.1], with $\{\alpha\} \equiv (q_1, q_2)$, where we restrict ourselves to the 1D case. The corresponding bi-photon wavefunction is given by,

$$\phi(q_1, q_2) = \int d\Omega_p \exp\left(-\left(\frac{\Omega_p}{2\sigma}\right)^2\right)\phi(q_1, q_2, \Omega_p) \tag{5.1}$$

where,

$$\phi(q_1, q_2, \Omega_p) = \exp\left(-\frac{w_p^2}{4}(q_1 + q_2)^2\right)\text{sinc}(\frac{\Delta\tilde{k}_z(\Omega_p, T)L}{2})$$

and the phase-mismatch is given by ,

$$\Delta\tilde{k}_z = \Delta\tilde{k}_{coll} + D_+\Omega_p + \frac{(q_1 - q_2)^2}{4k_p} \tag{5.2}$$

Similar to the case described in the theory section, we need the detection field operator to deterimine the correlation functions when the frequency label of the PDC state can be ignored. In this case it can be defined as,

$$\hat{E}(x,z) \equiv \frac{1}{\sqrt{2\pi}} \int dq f_{spat}(q) e^{i(qx - \frac{q^2 z}{2k_p})} \hat{a}(q) \tag{5.3}$$

Now using the standard beam-splitter transformation equations as defined before and the following commutation algebra,

$$[\hat{a}(q_1), \hat{a}^{\dagger}(q_2)] = \delta(q_1 - q_2) \tag{5.4}$$

the second-order correlation function is given by

$$\begin{aligned} G^{(1)}(x_1,z_1) =& \langle \hat{E}_3^{\dagger}(x_1,z_1) \hat{E}_3(x_1,z_1) \rangle & (5.5)\\ =& (S_2^{\mathrm{I}} + S_4^{\mathrm{I}}) \int dq_2 \Big| \Theta(x_1,z_1,q_2) \Big|^2 + \\ & S_4^{\mathrm{II}} \int dq_1 \Theta^{(1)}(x_1,z_1,q_2) \Theta^{(2)}(x_1,z_1,q_2) & (5.6) \end{aligned}$$

where,
$S_2^{\mathrm{I}} = 2R|B|^2$, $S_4^{\mathrm{I}} = 8R|C|^2\Gamma$ and $S_4^{\mathrm{II}} = 16R|C|^2$
$\phi(q_1,q_2)$ is the product of the spatial filter f_{spat} with Eqn.[2.2] and,

$$\Theta^{(1)}(x_1,z_1,q_2) = \int dq_1 \Theta(x_1,z_1,q_1) \phi^*(q_1,q_2) \tag{5.7}$$

$$\Theta^{(2)}(x_1,z_1,q_2) = \int dq_1 [\Theta(x_1,z_1,q_1)]^* \phi(q_1,q_2) \tag{5.8}$$

$$\Theta(x_1,z_1,q_2) = \frac{1}{\sqrt{2\pi}} \int dq_1 e^{i(q_1 x_1)} \left[\phi(q_1,q_2) e^{-\frac{iq_1^2 z_1}{2k}} \right] \tag{5.9}$$

Similarly the fourth-order correlation function,

$$G^{(2)}(x_1,z_1,x_2,z_2) = (D_2^{\mathrm{I}} + D_4^{\mathrm{I}}) \Big| \Theta^{2D}(x_1,x_2,z_1,z_2) \Big|^2 + D_4^{\mathrm{II}} \Bigg[\int dq_2 |\Theta(x_1,z_1,q_2)|^2 . \int dq_1 |\Theta(x_2,z_2,q_1)|^2 \Bigg] + D_4^{\mathrm{II}} \Bigg[\int dq_1 \Theta^*(x_1,z_1,q_1) \Theta(x_2,z_2,q_1) \Bigg]^2 \tag{5.10}$$

where,
$D_2^{\mathrm{I}} = 2TR|B|^2$, $D_4^{\mathrm{I}} = 8\Gamma|C|^2$, $D_4^{\mathrm{II}} = 8TR|C|^2$ and

$$\Theta^{2D}(x_1, x_2, z_1, z_2) = \frac{1}{2\pi} \int dq_1 dq_2 e^{i(q_1 x_1 + q_2 x_2)} \left[\phi(q_1, q_2) e^{-i(\frac{q_1^2 z_1}{2k_p} + \frac{q_2^2 z_2}{2k_p})} \right] \tag{5.11}$$

and sixth-order correlation is given by

$$G^{(3)}(x_1, x_2, z_1, z_2) = 8|TC|^2 R_1 T_1 R \Big[2|\Theta^{2D}(x_1, x_2, z_1, z_2)|^2 \int dq_4 |\Theta(x_2, q_4, z_2)|^2 + |\Theta^{2D}(x_2, x_2, z_2, z_2)|^2 \int dq_4 |\Theta(x_1, q_4, z_1)|^2 \Big] \tag{5.12}$$

The independent fourth-order correlation function is given by a product of two second-order correlation functions corresponding to D1 and D2. This contribution is given by,

$$G_{ind}^{(2)}(x_1, x_2, z_1, z_2) = G^{(1)}(x_1, z_1) G^{(1)}(x_2, z_2) \tag{5.13}$$

Likewise the independent sixth-order correlation function is given by,

$$G_{ind}^{(3)}(x_1, x_2, z_1, z_2) = G^{(2)}(x_2, x_2, z_2, z_2) G^{(1)}(x_1, z_1) \tag{5.14}$$

Note that experimentally we impose $x_2 = x_3$ and $z_1 = z_2 = z$.
The net two-folds as described in the theory are,

$$G_{net}^{(2)}(x_1, z_1, x_2, z_2) = 2G^{(2)}(x_1, z_1, x_2, z_2) - G_{ind}^{(2)}(x_1, x_2, z_1, z_2) \tag{5.15}$$

and likewise the net three-folds are given by,

$$G_{net}^{(3)}(x_1, x_2, z_1, z_2) = 2G^{(3)}(x_1, x_2, z_1, z_2) - G_{ind}^{(3)}(x_1, x_2, z_1, z_2) \tag{5.16}$$

Chapter 6

Appendix 2

Here we briefly mention our approach for normalizing the down-converted state. This is important if we want to subtract the correlations from the independent contribution in a coherent manner.

$$|\psi\rangle \equiv |\psi\rangle^{PDC} = A\,|vac\rangle + B\,|\psi_2\rangle + C\,|\psi_4\rangle \tag{6.1}$$

where,
$|\psi_2\rangle$ and $|\psi_4\rangle$ are short hand notations for the two-photon and the four-photon state
$A \equiv 1 - B^2\Gamma - 12C^2\Gamma^2$, as defined before
$C = B^2/2$ and
$\Gamma = \int d\{\alpha\}\,|\phi\{\alpha\}|^2$ with $\{\alpha\} \equiv (q_1, q_2)$

We set $\Gamma = 1$ and redefine the PDC state as

$$|\tilde{\psi}\rangle \equiv \frac{|\psi\rangle}{\sqrt{\langle\psi|\psi\rangle}} \tag{6.2}$$

Note that this approach of normalizing the state is not unique and by no means the only way to normalize it. For instance, one can do the same for $A \equiv 1 - B^2\Gamma$.

Chapter 7

Appendix 3

Here we briefly explain how the theoretical plots were obtained. The false color plot in Fig. 7.1, (left) are the three-fold coincidences obtained by making use of Eqn. 2.35. The horizontal contribution visible in the figure corresponds to the case when there are two photons in the same spatial mode (at the center) and the independent third photon could be detected at either x_1 or $-x_1$. The false color plot on the right is the corrected or the net three-fold coincidences after subtracting the contribution of the independent pairs to the three-fold coincidence. The subtraction was carried out using Eqn.2.38. Note that the independent pairs allow for the correlations to be along the diagonal as well. After subtracting the correlations of the independent pairs from the three-fold coincidences we numerically set the negative values so obtained to zero, the reason being that these do no show up as appreciably in our experiment. This is attributed to the fact that these negative correlations are probably overshadowed by the noise in our experiment. The two faint spots that are barely visible are treated as a numerical artifact and are neglected in all our analysis. The theoretical plots shown in Figures 3.4 and 3.5 are obtained by a clockwise rotation of 45° of the net three-folds plotted in Fig. 7.1.

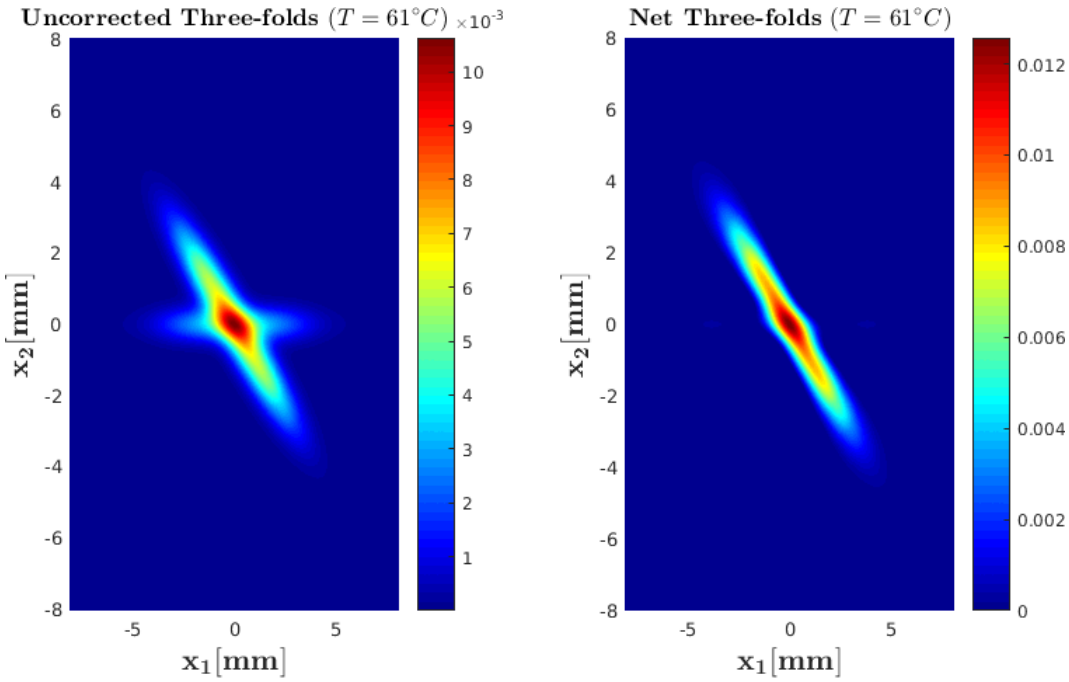

Figure 7.1: *Calculated three-fold coincidences without subtracting the contribution from independent pairs (left) and three-fold coincidences after the subtraction (right).*

Bibliography

[1] A. Einstein, B. Podolsky, and N. Rosen, "Can quantum-mechanical description of physical reality be considered correct?," *Physical Review*, vol. 47, pp. 777–780, 1935.

[2] S. Walborn, C. Monken, S. Pádua, and P. Souto Ribeiro, "Spatial correlations in parametric down-conversion," *Physics Reports*, vol. 495, no. 4, pp. 87–139, 2010.

[3] Z. Y. Jeff Ou, *Multi-Photon Quantum Interference*. USA: Springer US, 1st ed., 2007.

[4] R. Hambury Brown and R. Q. Twiss, "Correlation between photons in two coherent beams of light," *Nature*, vol. 177, no. 1, pp. 27–32, 1956.

[5] Z. Ou, J.-K. Rhee, and L. Wang, "Photon bunching and multiphoton interference in parametric down-conversion," *Physical Review A*, vol. 60, no. 1, pp. 593–604, 1999.

[6] Z. Ou, J.-K. Rhee, and L. Wang, "Observation of Four-Photon Interference with a Beam Splitter by Pulsed Parametric Down-Conversion," *Physical Review Letters*, vol. 83, no. 5, pp. 959–962, 1999.

[7] S. Ç. Yorulmaz, *Beyond photon pairs*. PhD Thesis, Leiden University, 2014.

[8] C. K. Hong and L. Mandel, "Theory of parametric frequency down conversion of light," *Physical Review A*, vol. 31, no. 4, pp. 2409–2418, 1985.

[9] R. W. Boyd, *Nonlinear Optics*. Academic Press, 3rd ed., 2008.

[10] T. Keller and M. Rubin, "Theory of two-photon entanglement for spontaneous parametric down-conversion driven by a narrow pump pulse," *Physical Review A*, vol. 56, no. 2, pp. 1534–1541, 1997.

[11] W. H. Peeters, *Two-photon interference: spatial aspects of two-photon entanglement, diffraction, and scattering*. PhD Thesis, Leiden University, 2010.

[12] J. Carmiggelt, M. D. Dood, and T. Oosterkamp, *Creating spatially entangled 4-photon states by Parametric Down Conversion*. B.Sc Thesis, Leiden University, 2016.

[13] H. de Riedmatten, V. Scarani, I. Marcikic, A. Acin, W. Tittel, H. Zbinden, and N. Gisin, "Two independent photon pairs versus four-photon entangled states in parametric down conversion," *Journal of Modern Optics*, vol. 51, no. 11, pp. 1637–1649, 2004.

[14] L. Mandel and E. Wolf, *Optical Coherence and Quantum Optics*. Cambridge University Press, 1995.

[15] B. Boulanger, I. Rousseau, J. P. Fève, M. Maglione, B. Ménaert, and G. Marnier, "Optical Studies of Laser-Induced Gray-Tracking in KTP," *IEEE Journal of Quantum Electronics*, vol. 35, no. 3, pp. 281–286, 1999.

[16] B. Boulanger, M. M. Fejer, R. Blachman, and P. F. Bordui, "Study of KTiOPO4 gray-tracking at 1064, 532, and 355 nm," *Applied Physics Letters*, vol. 65, no. 19, pp. 2401–2403, 1994.

[17] *Raicol Crystals: Non-linear, Electrooptic Crystals And Elements Catalogue*.

[18] P. E. Powers, *Field Guide to Nonlinear Optics*. USA: SPIE, 2013.

[19] D. B. Horoshko, G. Patera, A. Gatti, and M. I. Kolobov, "X-entangled biphotons: Schmidt number for 2D model," *European Physical Journal D*, vol. 66, no. 9, 2012.

[20] A. Christ, K. Laiho, A. Eckstein, K. N. Cassemiro, and C. Silberhorn, "Probing multimode squeezing with correlation functions," *New Journal of Physics*, vol. 13, 2011.

[21] A. J. H. Van Der Torren, S. C. Yorulmaz, J. J. Renema, M. P. Van Exter, and M. J. A. De Dood, "Spatially entangled four-photon states from a periodically poled potassium-titanyl-phosphate crystal," *Physical Review A*, vol. 85, no. 4, 2012.

[22] L. Mandel, "Physical significance of operators in quantum optics," *Physical Review*, vol. 136, no. 4B, pp. 1221–1224, 1964.

[23] S. P. Walborn and C. H. Monken, "Transverse spatial entanglement in parametric down-conversion," *Physical Review A*, vol. 76, no. 6, 2007.